RESEARCH ARTICLE

An Empirical Antigen Selection Method Identifies Neoantigens That Either Elicit Broad Antitumor T-cell Responses or Drive Tumor Growth

Hubert Lam[1], Lisa K. McNeil[1], Hanna Starobinets[1], Victoria L. DeVault[1], Roger B. Cohen[2], Przemyslaw Twardowski[3], Melissa L. Johnson[4], Maura L. Gillison[5], Mark N. Stein[6], Ulka N. Vaishampayan[7], Arthur P. DeCillis[1], James J. Foti[1], Vijetha Vemulapalli[1], Emily Tjon[1], Kyle Ferber[1], Daniel B. DeOliveira[1], Wendy Broom[1], Parul Agnihotri[1], Elizabeth M. Jaffee[8], Kwok-Kin Wong[9], Charles G. Drake[6], Pamela M. Carroll[1], Thomas A. Davis[1], and Jessica Baker Flechtner[1]

ABSTRACT Neoantigens are critical targets of antitumor T-cell responses. The ATLAS bioassay was developed to identify neoantigens empirically by expressing each unique patient-specific tumor mutation individually in *Escherichia coli*, pulsing autologous dendritic cells in an ordered array, and testing the patient's T cells for recognition in an overnight assay. Profiling of T cells from patients with lung cancer revealed both stimulatory and inhibitory responses to individual neoantigens. In the murine B16F10 melanoma model, therapeutic immunization with ATLAS-identified stimulatory neoantigens protected animals, whereas immunization with peptides associated with inhibitory ATLAS responses resulted in accelerated tumor growth and abolished efficacy of an otherwise protective vaccine. A planned interim analysis of a clinical study testing a poly-ICLC adjuvanted personalized vaccine containing ATLAS-identified stimulatory neoantigens showed that it is well tolerated. In an adjuvant setting, immunized patients generated both $CD4^+$ and $CD8^+$ T-cell responses, with immune responses to 99% of the vaccinated peptide antigens.

SIGNIFICANCE: Predicting neoantigens *in silico* has progressed, but empirical testing shows that T-cell responses are more nuanced than straightforward MHC antigen recognition. The ATLAS bioassay screens tumor mutations to uncover preexisting, patient-relevant neoantigen T-cell responses and reveals a new class of putatively deleterious responses that could affect cancer immunotherapy design.

INTRODUCTION

The clinical benefit of immune checkpoint inhibitor (ICI) therapies in cancer provides evidence that the immune system can control and even eradicate tumors (1). The effectiveness of ICI therapies relies primarily on T-cell recognition of neoantigens derived from tumor-specific mutations (2–4). Cancer vaccines based on these neoantigens have the potential to target a broad array of targets by increasing the pool of neoantigen-specific $CD4^+$ and $CD8^+$ T cells, which may limit metastatic tumor escape. Both T-cell subsets have clear importance in controlling tumor growth (5, 6). Moreover, $CD4^+$ T-cell support during priming is critical for secondary expansion and effector function of $CD8^+$ T-cell responses (7). Successful generation of immunity against cancer neoantigens has the potential to increase the efficacy of ICI therapies while being safe and well tolerated.

The feasibility of personalized neoantigen cancer vaccines was recently demonstrated in two independent clinical trials in which computational methods were used to predict MHC class I antigens from large numbers of neoantigen candidates (8, 9). In these studies, 20% or fewer of the neoantigens selected as MHC class I epitopes were immunogenic for $CD8^+$ T cells when measured directly *ex vivo* after vaccination. Most of the responses were measured in the $CD4^+$ T-cell subset despite having been predicted as $CD8^+$ T-cell antigens (10). *In silico* prediction for MHC class II antigen identification presents multiple challenges including polymorphisms in the class II molecules, variations in epitope length, the influence of peptide flanking regions, and challenges in the identification of the correct binding core (11). Even if computational methods correctly predict MHC antigen presentation, antigens selected by this approach may still fail because the patient's T-cell repertoire cannot respond to the antigen *in vivo*.

To overcome the challenges associated with *in silico* neoantigen prediction, we developed ATLAS, a robust *ex vivo* platform that empirically identifies neoantigens to which a subject has already generated an immune response (12). With this HLA-agnostic bioassay, each putative antigen is expressed individually in *Escherichia coli*, with or without a coexpressed cytolysin to facilitate MHC class I or class II processing, respectively (13). The *E. coli* library is fed in an ordered array to autologous dendritic cells derived from each patient's peripheral blood and incubated overnight with their T cells. If the T cells recognize their cognate antigen, they will secrete measurable cytokines. ATLAS has previously yielded novel antigens with clinical efficacy when administered as a vaccine against infectious diseases (14–16), but has not been previously applied to patients with cancer, or to immunologically competent murine cancer models.

Here, we report preclinical and clinical results demonstrating that ATLAS accurately identifies neoantigens that drive both stimulatory and inhibitory T-cell responses to cancer, as defined by inflammatory cytokine secretion. Many identified neoantigens did not fit common selection criteria for *in silico* neoantigen selection. Therapeutic vaccination of mice with ATLAS-identified stimulatory neoantigens resulted in antitumor efficacy as a monotherapy. By contrast, vaccines

[1]Genocea Biosciences Inc., Cambridge, Massachusetts. [2]University of Pennsylvania, Philadelphia, Pennsylvania. [3]John Wayne Cancer Institute, Santa Monica, California. [4]Sarah Cannon Research Institute, Nashville, Tennessee. [5]The University of Texas MD Anderson Cancer Center, Houston, Texas. [6]Columbia University Medical Center, New York, New York. [7]Karmanos Cancer Institute, Detroit, Michigan. [8]Johns Hopkins School of Medicine, Baltimore, Maryland. [9]NYU Langone Health, New York, New York.

Note: Supplementary data for this article are available at Cancer Discovery Online (http://cancerdiscovery.aacrjournals.org/).

Corresponding Author: Jessica Baker Flechtner, Genocea Biosciences, 100 Acorn Park Drive, Cambridge, MA 02140. E-mail: jessica.flechtner@genocea.com

Cancer Discov 2021;11:696–713

doi: 10.1158/2159-8290.CD-20-0377

Table 1. HLA types, mutations, and ATLAS responses for the research cohort

	HLA haplotypes		Mutations		Stimulatory responses		Inhibitory responses	
	MHC class I	MHC class II	S	NS	CD8+	CD4+	CD8+	CD4+
USO-004	A 01:01, 02:01 B 08:01, 15:01 C 07:01, 04:01	DPA1*01:03, 01:03; DPB1*04:01, 03:01; DQA1*01:02, 01:02; DQB1*06:02, 04:02; DRA1*01:01, 01:01; DRB1*15:01, 08:01	700	181	0%	12%	0%	12%
USO-007	A 02:01, 11:01 B 35:01, 15:01 C 03:04, 04:01	DPA1*01:03, 01:03; DPB1*04:02, 03:01; DQA1*01:02, 01:02; DQB1*06:04, 05:02; DRA1*01:01, 01:01; DRB1*13:02, 01:01	971	130	0%	0%	1%	3%
USO-008	A 01:01, 24:02 B 08:01, 15:01 C 03:03, 07:01	DPA1802:01, 02:01; DPB1*39:01, 04:01; DQA1*05:01, 05:01; DQB1*03:01, 02:01; DRA1*01:01, 01:01; DRB1*11:01, 03:01	170	57	0%	9%	0%	0%
USO-010	A 02:01, 02:05 B 07:05, 50:01 C 06:02, 15:05	DPA1*01:03, 01:03; DPB1*03:01, 04:01; DQA1*02:01, 03:01; DQB1*03:02, 02:01; DRA1*01:01, 01:01; DRB1*04:05, 07:01	734	97	0%	0%	0%	1%
USO-013	A 03:01, 33:03 B 15:16, 35:01 C 04:01, 14:02	DPA1*03:02, 03:02; DPB1*04:01, 17:01; DQA1*01:02, 02:01; DQB1*05:01, 02:01; DRA1*01:01, 01:01; DRB1*13:02, 07:01	765	176	1%	3%	0%	0%
USO-027	A 11:01 B 14:02, 51:01 C 03:03, 08:02	DPA1*01:03, 01:03; DPB1*02:01, 34:01; DQA1*01:03, 05:01; DQB1*06:01, 03:01; DRA1*01:01, 01:01; DRB1*15:02, 11:01	84	17	2%	5%	2%	0%
USO-028	A 24:02, 68:01 B 35:03, 51:01 C 04:01, 15:02	DPA1*01:03, 01:03; DPB1*02:01, 04:01; DQA1*01:03, 01:03; DQB1*06:11, 06:11; DRA1*01:01, 01:01; DRB1*15:01, 13:01	931	319	2%	5%	2%	3%
USO-031	A 02:01, 02:05 B 50:01, 51:01 C 06:02, 14:02	DPA1*01:03, 01:03; DPB1*03:01, 02:01; DQA1*01:03, 02:01; DQB1*06:03, 06:03; DRA1*01:01, 01:01; DRB1*13:01, 07:01	215	69	21%	25%	5%	4%
USO-041	A 01:01, 03:01 B 07:02, 08:01 C 07:01, 07:02	DPA1*01:03, 01:03; DPB1*02:01, 04:01; DQA1*01:02, 03:01; DQB1*06:02, 03:02; DRA1*01:01, 01:01; DRB1*04:04, 15:01	222	63	35%	0%	1%	5%
Median			700	97	1%	5%	1%	3%

Abbreviations: NS, nonsynonymous; S, synonymous.

that included even a single neoantigen associated with inhibitory responses in ATLAS led to accelerated tumor outgrowth and/or abrogation of vaccine-mediated protection. We have termed these inhibitory antigens "Inhibigens"; they are defined as antigens to which inflammatory T-cell cytokine secretion is suppressed to levels below baseline. These studies demonstrate the feasibility of using an *ex vivo* antigen detection method to formulate patient-specific cancer vaccines and demonstrate the potential importance of distinguishing between stimulatory and inhibitory antigens in a treatment or prevention setting.

RESULTS

ATLAS: Identification of Neoantigens and Inhibigens in Patients with Lung Cancer

A cohort of nine patients with lung cancer was recruited into an observational study to assess preexisting neoantigen-specific T-cell responses using the ATLAS assay. Patient demographics, HLA haplotypes, and prior treatment are summarized in Table 1, Supplementary Fig. S1A and S1B, and Supplementary Table S1, respectively. Tumor sequencing identified between 84 and 971 somatic variants per patient, with a median of 700. In total, 1,015 unique mutations were profiled: 934 variants for $CD8^+$ T-cell responses and 525 variants for $CD4^+$ T-cell responses (Table 1; Supplementary Table S2). The median number of mutations classified as immunologically recognized stimulatory neoantigens based on the ATLAS assay was low, with 5% and 1% of the screened mutations for $CD4^+$ and $CD8^+$ T cells, respectively. Surprisingly, many neoantigen-specific T-cell responses were inhibitory, defined as downregulating IFNγ and/or TNFα cytokine secretion to levels significantly below baseline controls. Inhibitory responses were observed to a median of 3% and 1% of mutations for $CD4^+$ and $CD8^+$ T cells, respectively (Fig. 1A; Table 1).

Using the developer's recommended 2% cutoff (17), only 6% of the epitopes predicted by NetMHCpan and none of the epitopes predicted by NetMHCIIpan elicited a stimulatory T-cell response in the ATLAS assay (Fig. 1B). Moreover,

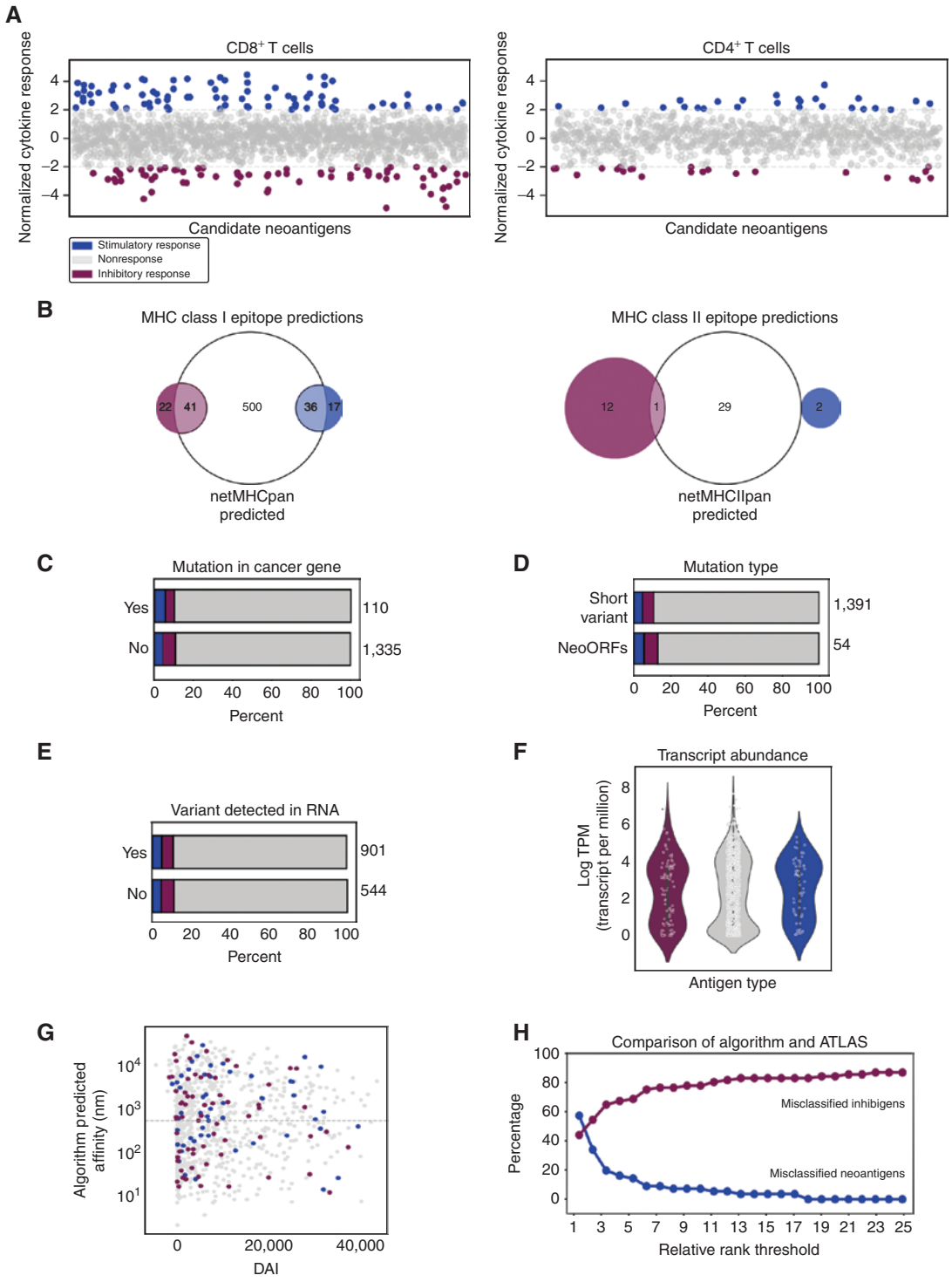

Figure 1. CD4+ and CD8+ T-cell responses in ATLAS and the neoantigen characteristics. **A,** Normalized cytokine responses for IFNγ and TNFα across 9 lung cancer subjects and 1,015 unique mutations profiled. Each point represents the average (of two) observed cytokine response for a given analyte for each mutation profiled in ATLAS normalized to the negative control responses. Horizontal line indicates the statistical cutoff for determination of stimulatory (blue) or inhibitory (burgundy) T-cell responses. **B,** Venn diagrams comparing ATLAS-identified T-cell responses with NetMHCpan 4.0 (934 putative neoantigens) or NetMHCIIpan 4.0 (525 putative neoantigens) predictions using a 2% cutoff. Blue circles represent neoantigens, and burgundy circles represent Inhibigens. **C** and **D,** Relative proportion of neoantigens (blue), Inhibigens (maroon), and nonantigenic (gray) mutations classified by if the mutation is in a known cancer gene (**C**) or a short variant or a neoORF (**D**). **E,** Classification of responses by if the mutation was expressed as determined by RNA-seq analysis. **F,** Classification of responses by copy number. *y*-axis represents log transcripts per million, and *x*-axis indicates response determination by ATLAS. **G,** Minimum predicted affinity (nmol/L) plotted against the maximum calculated DAI for each SNV. **H,** The concordance between ATLAS and NetMHCpan/NetMHCIIpan algorithms for different algorithm thresholds. The red line shows the false positive rate defined as percentage of Inhibigens classified as antigens by the algorithm. The blue line shows the false negative rate defined as the percentage of neoantigens missed by the algorithm.

32% of the neoantigens identified by ATLAS to elicit CD8$^+$ T-cell IFNγ and/or TNFα secretion were not predicted by algorithms. In this cohort of patients, 7% of the NetMHCpan-predicted antigens were identified as Inhibigens, demonstrating that current algorithms are unable to distinguish between neoantigens and Inhibigens, as algorithms predict only peptide binding to specific MHC/HLA and are not designed to predict the immune response to the peptide. Therefore, these algorithms may result in the inadvertent prioritization of potentially deleterious targets. Next, common criteria used for *in silico* predictions were assessed to determine if any could enrich for mutations that elicited patient T-cell responses in ATLAS. Neoantigens and Inhibigens identified using the ATLAS assay were not enriched for known cancer genes (Fig. 1C), or novel sequences (indels, frameshifts, neoORFs) preferentially over short variants [single-nucleotide variants (SNV) Fig. 1D], nor were all ATLAS-identified neoantigens expressed as determined by RNA-sequencing (RNA-seq) analysis, which measures only genes that are actively transcribed at the time of collection and in the specific portion of tumor that is biopsied (Fig. 1E). Furthermore, there was no relationship between transcript abundance and antigenicity (Fig. 1F). The differential predicted affinity of the mutated versus wild-type antigen for the MHC molecule, measured by use of the differential agretopic index (DAI), was not different for either stimulatory neoantigens or Inhibigens (Fig. 1G). Finally, we tested whether reducing the stringency of the NetMHCpan cutoff would lead to predictions consistent with those detected by ATLAS. Although reducing the binding affinity threshold did decrease neoantigens missed by the algorithm, the proportion of Inhibigens also increased (Fig. 1H). Therefore, the ATLAS bioassay empirically identifies neoantigens in peripheral blood of patients with cancer that are not predicted with *in silico* methods and distinguishes putative antigens based on their ability to stimulate or inhibit T-cell responses *ex vivo*.

Characterizing T-cell Responses to Neoantigens or Inhibigens in a Murine Model of Melanoma

To determine if the neoantigens identified using ATLAS were biologically relevant, the ATLAS *ex vivo* assay was applied to the B16F10 murine melanoma model. Whole-exome sequencing of B16F10 melanoma tumors resected from C57BL/6 mice identified 1,679 nonsynonymous mutations, exceeding the 962 previously reported (18) and in line with more recent sequencing of B16F10 (Supplementary Table S3; ref. 19). An ATLAS library expressing each individual mutation was constructed and used to screen CD8$^+$ T cells from the spleens of tumor-bearing mice, resulting in the identification of 66 neoantigens and 57 Inhibigens (Fig. 2A; Supplementary Table S3). A lead neoantigen candidate, Gal3St1$_{P64A}$ (galactose-3-O-sulfotransferase; Supplementary Table S2), was selected for further study based on high IFNγ and TNFα secretion in multiple mouse ATLAS screens. Although the Gal3St1$_{P64A}$ mutation has been previously identified in B16F10 tumors (18, 19), neither immunogenicity nor efficacy has been described with formulations containing this sequence after vaccination.

When a vaccine containing three antigens—Gal3St1$_{P64A}$ and previously identified M30 (MHC II neoantigen; ref. 18) and TRP2 (MHC I tumor-associated antigen; ref. 20; Supplementary Table S4)—was therapeutically administered with adjuvant (CpG, QS21, and 3D-PHAD) to tumor-bearing mice, tumor growth was either significantly delayed or completely abrogated compared with controls (Fig. 2B). Gal3St1$_{P64A}$ as a single antigen vaccine conferred some protection (Supplementary Fig. S2), but a combination of all three antigens was necessary for maximal antitumor efficacy, supporting the concept that a multiantigen, CD8$^+$ and CD4$^+$ broad-spectrum T cell–targeted vaccine is necessary for protection in this aggressive model (21). Of note, the formulation containing the ATLAS-identified Gal3St1$_{P64A}$ neoantigen was significantly more protective than the published efficacious combination containing M27 (MHC I neoantigen; Fig. 2B; ref. 18). T-cell responses were generated to all vaccine antigens, with potent IFNγ responses measured to Gal3St1$_{P64A}$ (Fig. 2C). Cross-reactivity with wild-type Gal3St1 was not observed (Supplementary Fig. S3). Vaccinated mice that showed no evidence of tumor growth were rechallenged with B16F10 on day 63. As compared with age-matched naïve controls, mice previously vaccinated with the Gal3St1$_{P64A}$ vaccine had negligible tumor growth, confirming the generation of durable protective immunity (Fig. 2D).

The detection of Inhibigens by the ATLAS screen suggests potentially deleterious antigen-specific immune modulation by T cells, the biological relevance of which was evaluated by therapeutic vaccination with a pool of 27-mer synthetic long peptides (SLP) spanning four ATLAS-identified Inhibigens (Supplementary Table S4). In tumor-bearing mice, immunization with Inhibigen peptides led to a marked increase in tumor growth kinetics relative to mice that received adjuvant alone (Fig. 3A). Immune responses to Inhibigen peptide immunization, measured by IFNγ enzyme-linked immunosorbent spot (ELISpot) assays, were lower than those to stimulatory neoantigens (Supplementary Fig. S4). Flow cytometric analysis of progressing tumors revealed reduced T-cell infiltration, particularly by CD8$^+$ T cells, as compared with control tumors (Supplementary Fig. S5). When the pool of Inhibigen peptides was added to a formulation containing M30 and TRP2, protection conferred by T-cell responses to M30 and TRP2 was completely abrogated (Fig. 3B), suggesting that deleterious Inhibigen-specific responses can be dominant to protective responses. After deconvolution of the peptide pool to test each Inhibigen individually with M30 and TRP2, two Inhibigens were identified as primarily responsible for reduced efficacy. In particular, the Inhibigen peptide spanning the MMP9 frameshift mutation (MMP9$_{FS}$) completely abrogated protection (Fig. 3C). The TAAR9$_{C190W}$ Inhibigen also dampened protection but to a lesser extent, whereas ABCA17 and ASB14 Inhibigens had no demonstrable effect on tumor kinetics. The protumor effect of MMP9$_{FS}$ immunization correlated with a significant decrease in T-cell IFNγ secretion specific for protective M30 and TRP2 antigens administered in the same vaccine pool (Fig. 3D). In addition, CD8$^+$ T-cell infiltration into tumors was significantly diminished by MMP9$_{FS}$ immunization (Fig. 3E and F; Supplementary Fig. S6). Analysis of CD4$^+$CD25$^+$FOXP3$^+$ cells in the spleens of mice therapeutically immunized with a vaccine containing the MMP9$_{FS}$ SLP did not reveal significant cell number differences relative to mice that received the vaccine in the absence of MMP9$_{FS}$ (Fig. 3G). In addition, increases in

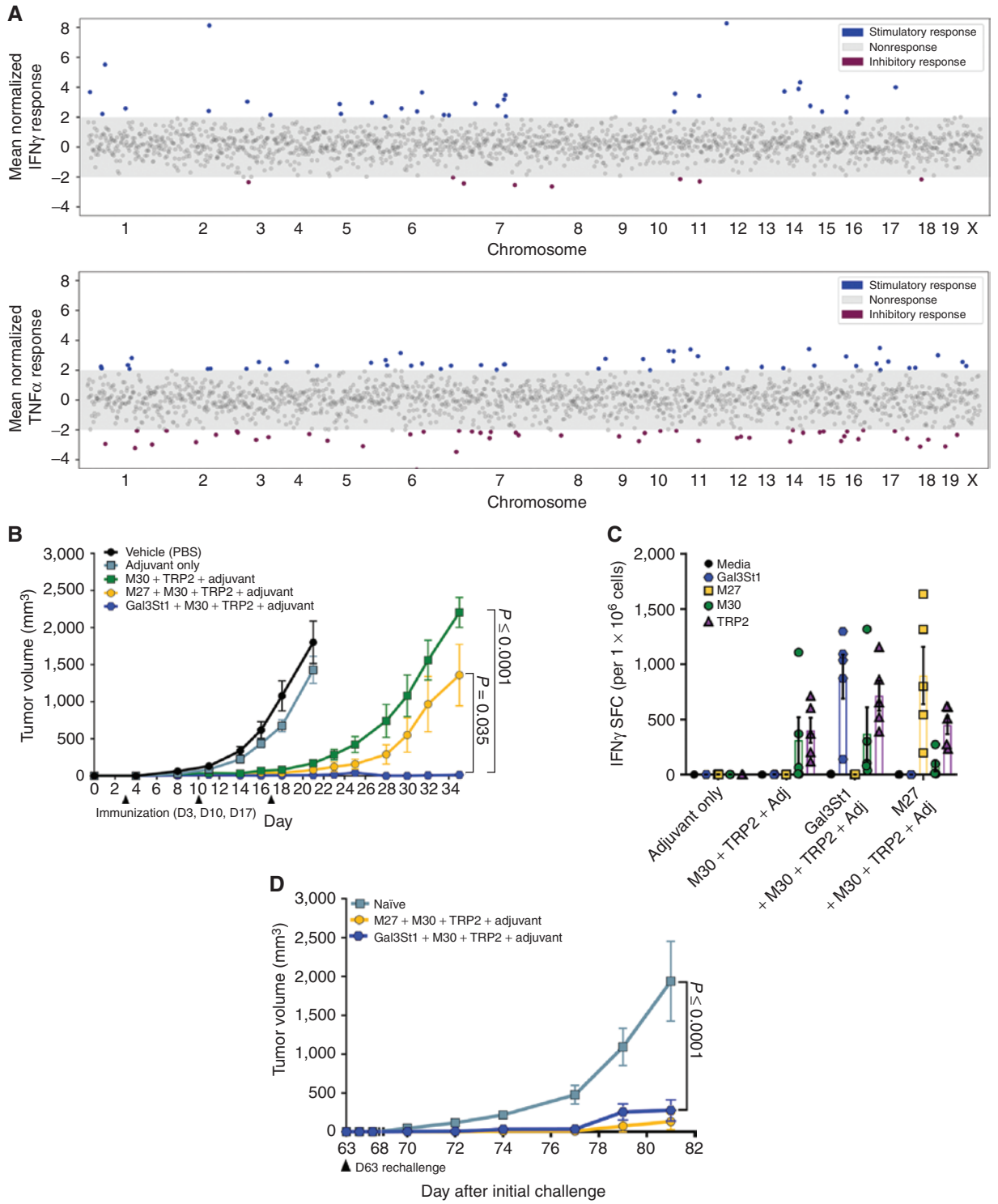

Figure 2. ATLAS identifies neoantigens and Inhibigens that affect tumor progression in mice. **A,** Normalized cytokine responses for IFNγ (top) and TNFα (bottom) to B16F10 candidate neoantigens in the ATLAS assay. Each point represents the average observed cytokine response for each mutation profiled in ATLAS. Horizontal lines indicate statistical cutoff for determination of neoantigen (blue) or Inhibigen (burgundy) T-cell responses. **B,** Mean tumor growth kinetics after therapeutic immunization with indicated neoantigen peptide vaccine ± adjuvant [CpG (5 μg), 3D-PHAD (5 μg), and QS21 (25 μg) on days 3, 10, and 17; $n \geq 9$ per group; ulcerated tumors censored from analysis]. *P* values at day 35 determined by one-way ANOVA. **C,** Antigen-specific immune response to neoantigen peptides by ELISpot analysis on mouse splenocytes on day 17. Each symbol represents the response from an individual mouse. **D,** Previously vaccinated mice that did not develop measurable tumors from Gal3St1 + M30 + TRP2 ($n = 5$) and M27 + M30 + TRP2 ($n = 2$) groups were rechallenged with B16F10 cells on day 63 after primary challenge, and mean tumor volume and SEM are plotted over time. Mice that developed small tumors (<100 mm^3) between days 35 and 62 were excluded from rechallenge. Naïve age-matched mice ($n = 9$) were challenged as a control. *P* value determined by *t* test at day 81.

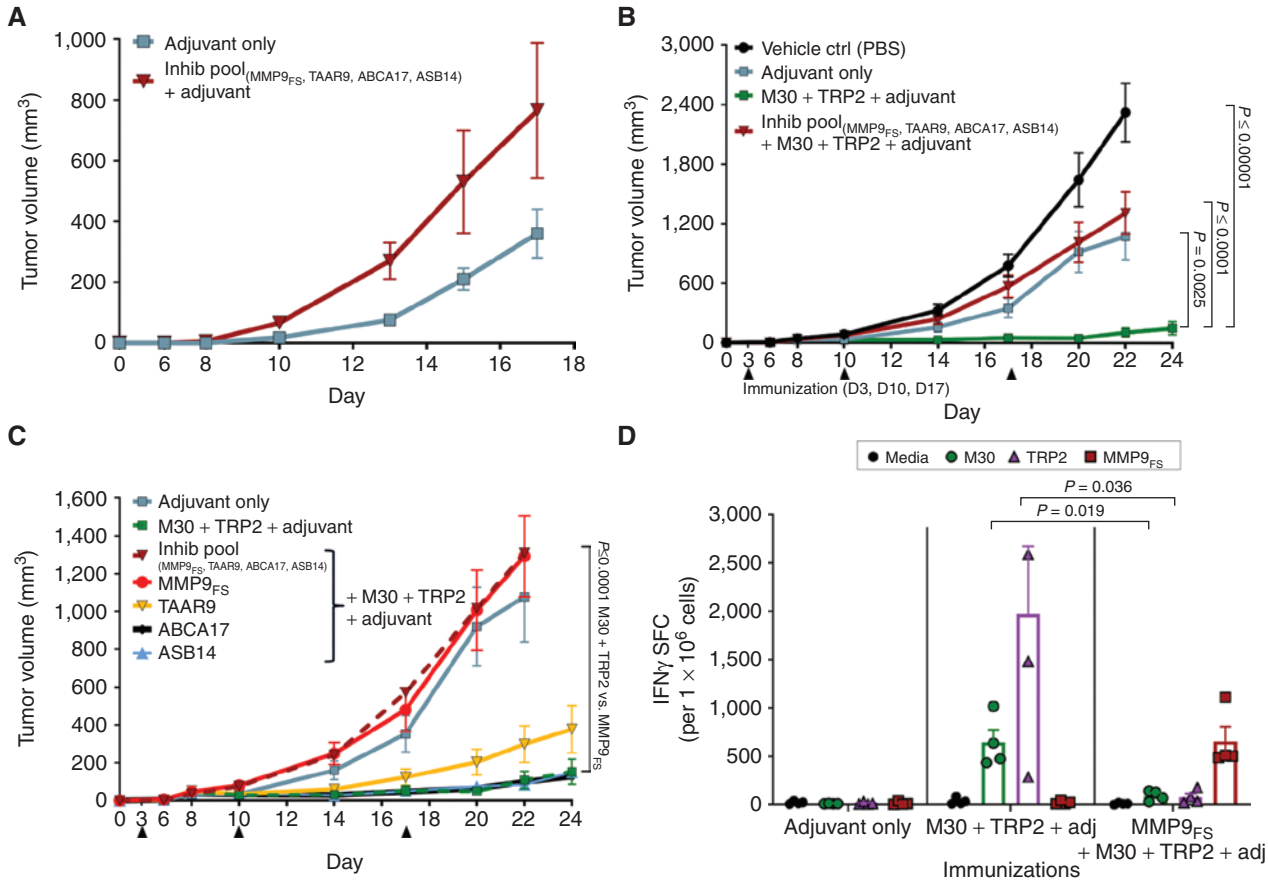

Figure 3. Vaccination with ATLAS-identified Inhibigens leads to accelerated tumor growth and abrogated efficacy of an otherwise protective vaccine. **A,** B16F10 mean tumor growth kinetics ± SEM after therapeutic immunization with an adjuvanted Inhibigen peptide vaccine or adjuvant alone ($n = 11$ per group). **B,** Mean tumor growth kinetics after therapeutic immunization with controls, or a combination of stimulatory neoantigens (2 SLPs) ± Inhibigen pool (4 SLPs) with adjuvant (CpG, QS21, and 3D-PHAD) or (**C**) the combination of two stimulatory SLPs with individual deconvoluted Inhibigen SLPs with adjuvant ($n = 15$ per group). Statistical analyses were performed by one-way ANOVA on day 22. **D,** Antigen-specific immune response to stimulatory or Inhibigen neoantigen SLPs by ELISpot analysis on splenocytes from vaccinated mice. Data are represented as mean ± SEM IFNγ spot-forming cells (SFC) per million splenocytes; each symbol represents one mouse. (*continued on following page*)

FOXP3$^+$ cells were not observed in the tumor microenvironment (TME) of Inhibigen-immunized mice by immunohistochemistry (IHC; Fig. 3F). Combined, these data suggest that differential expansion of conventional regulatory T cells (Treg) did not account for Inhibigen-induced phenotypic differences. Interestingly, a marked decrease in F4/80$^+$ and CD11c$^+$ cells in the TME was observed in Inhibigen-immunized mice, suggesting a differential effect on macrophage and/or dendritic cells in the tumor (Fig. 3F). Taken together, these data support the conclusion that the ATLAS approach detects both stimulatory and inhibitory antigens, and that including Inhibigens in a vaccine may lead to detrimental effects including decreased efficacy *in vivo*.

The ATLAS Approach in Patients: Analysis of Immunogenicity in the GEN-009-101 Clinical Trial

A planned interim analysis was performed on subjects participating in a phase I/IIa clinical trial that was designed to assess the safety and immunogenicity of ATLAS-identified neoantigens in a personalized vaccine for patients with melanoma, head and neck squamous cell cancer, urothelial carcinoma, or non–small cell lung cancer (NSCLC) who were without evidence of disease after initial therapy. Matched tumor and normal tissue from initial resection or biopsy were sequenced to identify the patient's unique mutanome followed by ATLAS screening (Supplementary Table S5). Neoantigens that elicited stimulatory CD4$^+$ or CD8$^+$ T-cell responses were included in the vaccine, and Inhibigens were excluded. Comprehensive ATLAS screening data across all patients are presented in Supplementary Table S5, and a representative patient screen is shown graphically in Supplementary Fig. S7. In the patient shown, stimulatory neoantigens were identified in both T-cell subsets, with 1 CD4$^+$ neoantigen and 15 CD8$^+$ neoantigens. In this patient, inhibitory responses were found in only the CD8$^+$ T-cell subset, whereas in other subjects, inhibitory responses were found in either one or both T-cell subsets (Table 2; Supplementary Table S5). As in the observational lung cancer cohort, there was no association of immunogenicity in ATLAS with DNA copy number, DAI, or

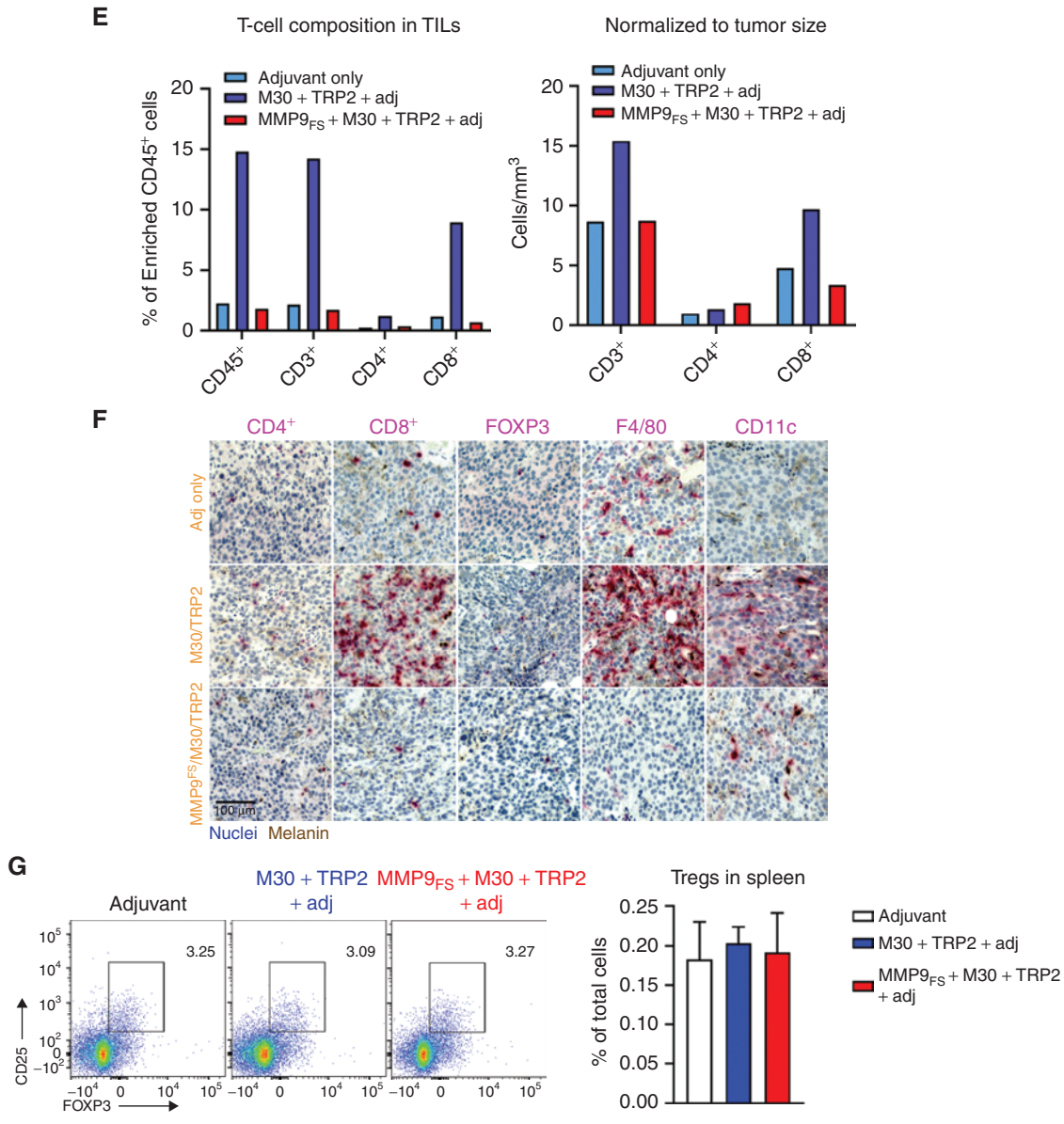

Figure 3. ***(Continued)*** **E,** Flow cytometric analysis of TILs isolated from vaccine-administered B16F10 tumor-bearing mice. Left, bar graph of proportion of CD45$^+$ T cells isolated from the TILs. Right, total CD3$^+$, CD4$^+$, and CD8$^+$ cells enriched from TIL normalized to tumor volume (mm^3). Analysis performed on tumor cells pooled from 4 mice/group. **F,** Immune cell populations assessed by chromogenic IHC of formalin-fixed, paraffin-embedded (FFPE) sections of B16F10 melanoma tumors. Stains shown are CD4$^+$, CD8$^+$, FOXP3, F4/80, and CD11c (pink). Nuclei were counterstained with hematoxylin (blue); natural B16F10 melanin deposits are visible (brown). Images are representative of multiple sections and tumors from each group. Scale bar, 100 µm. **G,** Flow cytometric analysis of Tregs in spleens of vaccinated animals ($n = 3$ animals per group). Representative plots gated on live CD3$^+$CD4$^+$ T cells and CD25$^+$ FOXP3$^+$ double-positive cells.

mutation type (short variant vs. neoORF; Supplementary Fig. S8A–S8H). Although there was a trend toward increased RNA expression of neoantigens versus nonantigens or Inhibigens, the correlation was low (Supplementary Fig. S8E). Not surprisingly for patients with cancer, there was significant interpatient variability in ATLAS outcomes with respect to frequency of stimulatory neoantigens and Inhibigens (Table 2). Application of NetMHCpan to patient-specific mutations was unable to predict most ATLAS-identified stimulatory neoantigens. Conversely, a number of Inhibigens identified by ATLAS would have been included in a NetMHCpan-directed vaccine (Supplementary Fig. S8H).

The clinical vaccine product, GEN-009, consists of 4 to 20 SLPs divided into 4 pools, with each pool containing 1 to 5 SLPs. A single pool was administered into each extremity combined with the adjuvant poly-ICLC (Hiltonol, Oncovir, Inc.). The vaccine was administered in a prime-boost schedule of five immunizations (Supplementary Fig. S9). Eight patients were vaccinated. One patient developed recurrent disease during vaccine manufacturing and therefore did not receive the

Table 2. Enrolled patients and ATLAS results

Patients	Age	Sex	Ethnicity	Tumor	Prior therapy	TMB (mutations/Mb)	Neoantigens	Inhibigens	Peptides in vaccine
A	53	F	White	Squamous NSCLC	Surgery/Carbo/Etop	0.18	6	0	10[a]
B	73	M	White	Urothelial carcinoma	Surgery/Mito Cis/Gem/Pembro	0.9	16	4	8
C	82	M	White	Melanoma	Surgery/Pembro/Ipi	8.16	199	41	16
D	48	M	White	Melanoma	Surgery	3.09	43	94	Recurrence prior to vaccination
E	64	M	White	Urothelial carcinoma	Surgery/Cis/Gem	0.88	18	1	13
F	66	F	White	NSCLC adenocarcinoma	Surgery	0.94	16	9	11
G	57	M	White	Bladder	Surgery	2.34	24	104	13
H	64	F	White	Urothelial carcinoma	Surgery/Cis/Gem	0.44	14	4	8
I	68	F	White	Urothelial carcinoma	Surgery/Gem	0.12	0	3	No stimulatory antigens
J	68	M	White	Bladder	Surgery	—	—	—	Insufficient tumor
K	68	M	White	SCCHN	Cetux/XRT	3.19	15	15	9
L	76	M	White	SCCHN	Carbo/Taxol/XRT	0.5	2	1	Insufficient antigens

Abbreviations: SCCHN, squamous cell carcinoma of the head and neck; Carbo, carboplatin; Cetux, cetuximab, Cis, cisplatin; Etop, etoposide; Gem, gemcitabine; ipi, ipilimumab; Mito, mitomycin-C; pembro, pembrolizumab; XRT, radiotherapy.

[a]Two peptides each for four deletion fragments positive in ATLAS.

vaccine (patient D). Interestingly, this subject had complete resection for stage IIIA melanoma without further adjuvant therapy but had a predominance of Inhibigens identified in their mutanome (Table 2). Patients for whom a vaccine was not feasible or who dropped out due to early progression were replaced. Supporting manufacturing feasibility, a GEN-009 personalized vaccine was generated for 100% of eligible patients, and the median overall time from tumor collection to vaccination was less than 16 weeks. To date, 37 vaccinations have been administered without a dose-limiting toxicity; adverse events were consistent with those expected from the adjuvant alone and were self-limited. These consisted of grade 1 injection site reactions/pain, fatigue, chills, headache, and influenza-like illness, with a single occurrence of grade 2 pyrexia. There were no clinically significant laboratory abnormalities. No patients have experienced disease recurrence after vaccination with a median follow-up of 34 weeks (range, 15–46 weeks), although one subject was diagnosed with a molecularly distinct second primary tumor while in the treatment period. Clinical follow-up of these patients is ongoing.

T-cell responses to the GEN-009 vaccine were analyzed by dual-color fluorospot assays in prevaccination and postvaccination samples. Pools of four overlapping peptides (OLP; 15 mer overlapping by 11 aa) were synthesized for each neoantigen SLP represented in the vaccine. Total peripheral blood mononuclear cells (PBMC) and sorted $CD4^+$ or $CD8^+$ T cells were evaluated for responsiveness to each of the individual immunized SLPs as well as vaccine pools. *Ex vivo* responses were assessed by IFNγ/Granzyme B (GrB) fluorospot assay. For the *in vitro* stimulation (IVS) assay, cells were expanded for 10 days with OLP pools and then assessed in an IFNγ/TNFα fluorospot assay. Comprehensive immunogenicity data for a single patient are shown in Fig. 4A–C. Modulation of neoantigen-specific $CD4^+$ and $CD8^+$ T-cell responses after vaccination was apparent by both *ex vivo* (plots A and B) and IVS (plot C) fluorospot. The responses varied for each immunized peptide, in some cases increasing after immunization and in other cases decreasing for a particular analyte. After vaccination, all patients had $CD4^+$ and $CD8^+$ T-cell responses to at least one peptide *ex vivo* (Fig. 4D; Supplementary Table S6). Across the cohort, most subjects had T-cell responses to a proportion of peptides included in their vaccine measurable *ex vivo* at baseline (Fig. 4D) and after IVS (Fig. 4E). Overall, there were immune responses detected to nearly all (99%) of the administered peptides (Fig. 4F; Supplementary Table S6).

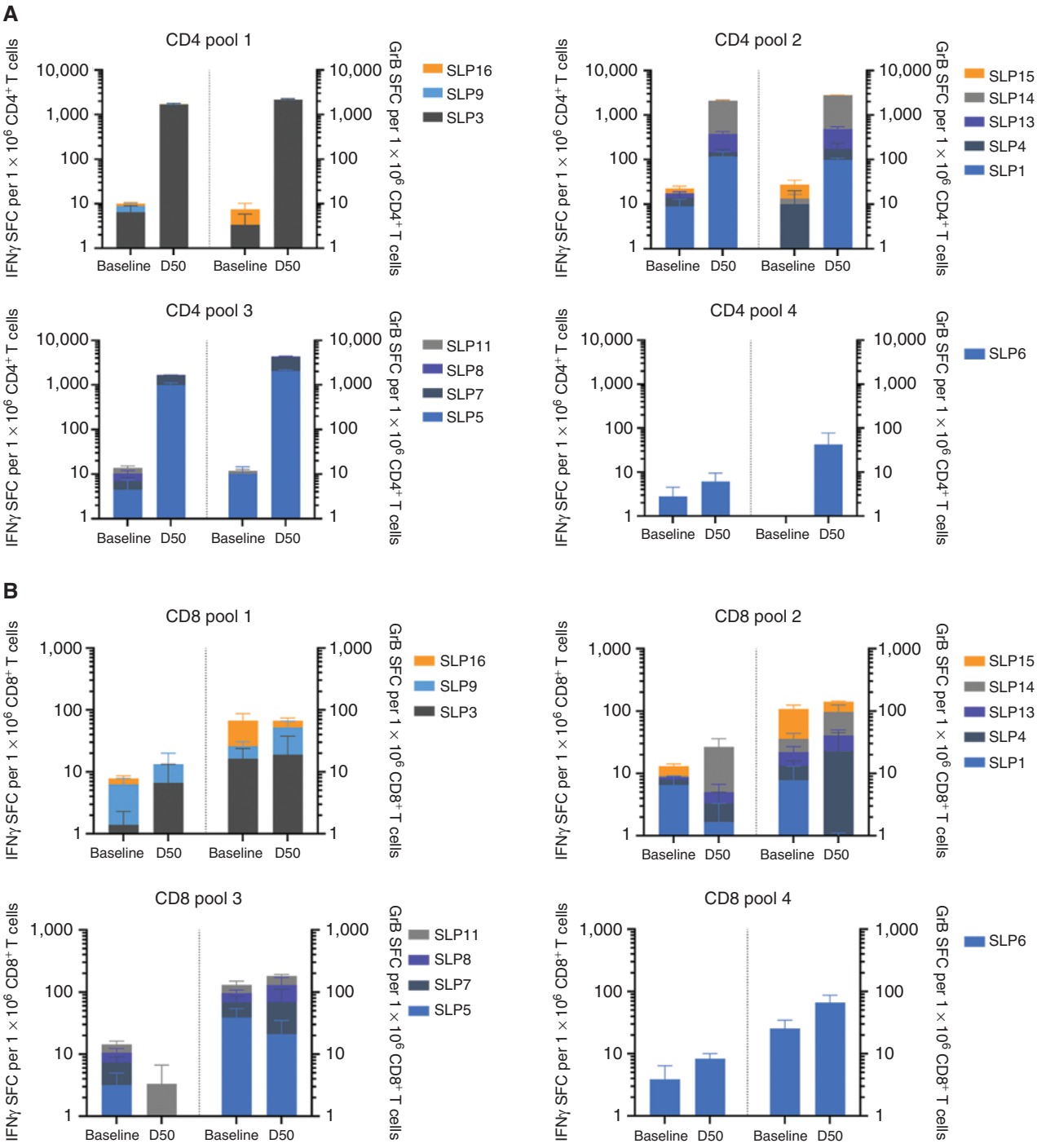

Figure 4. Vaccination elicits T-cell responses measurable by both *ex vivo* and IVS fluorospot. **A** and **B,** PBMCs from subject E were enriched for CD4+ or CD8+ T cells and stimulated with OLPs spanning each immunized SLP in an IFNγ and GrB dual-color *ex vivo* fluorospot assay. Data are reported as the background-subtracted mean SFC per million. Each plot represents the responses to the specific SLPs present in each of the four pools of immunization. (*continued on next page*)

Ex vivo neoantigen-specific CD4+ and CD8+ T-cell responses were identified to 51% and 41% of peptides, respectively. In addition, IVS CD4+ and CD8+ T-cell responses were observed against 87% and 59% of administered peptides, respectively. Responder analysis (statistical differences in magnitude after vaccination compared with baseline) revealed that on day 50, by the IFNγ assay, the magnitude of PBMC and CD4+ T-cell responses was statistically greater than responses at baseline for a median of 88% of SLPs; for CD8+ T-cell responses, increases were statistically significant for 63% of the SLPs

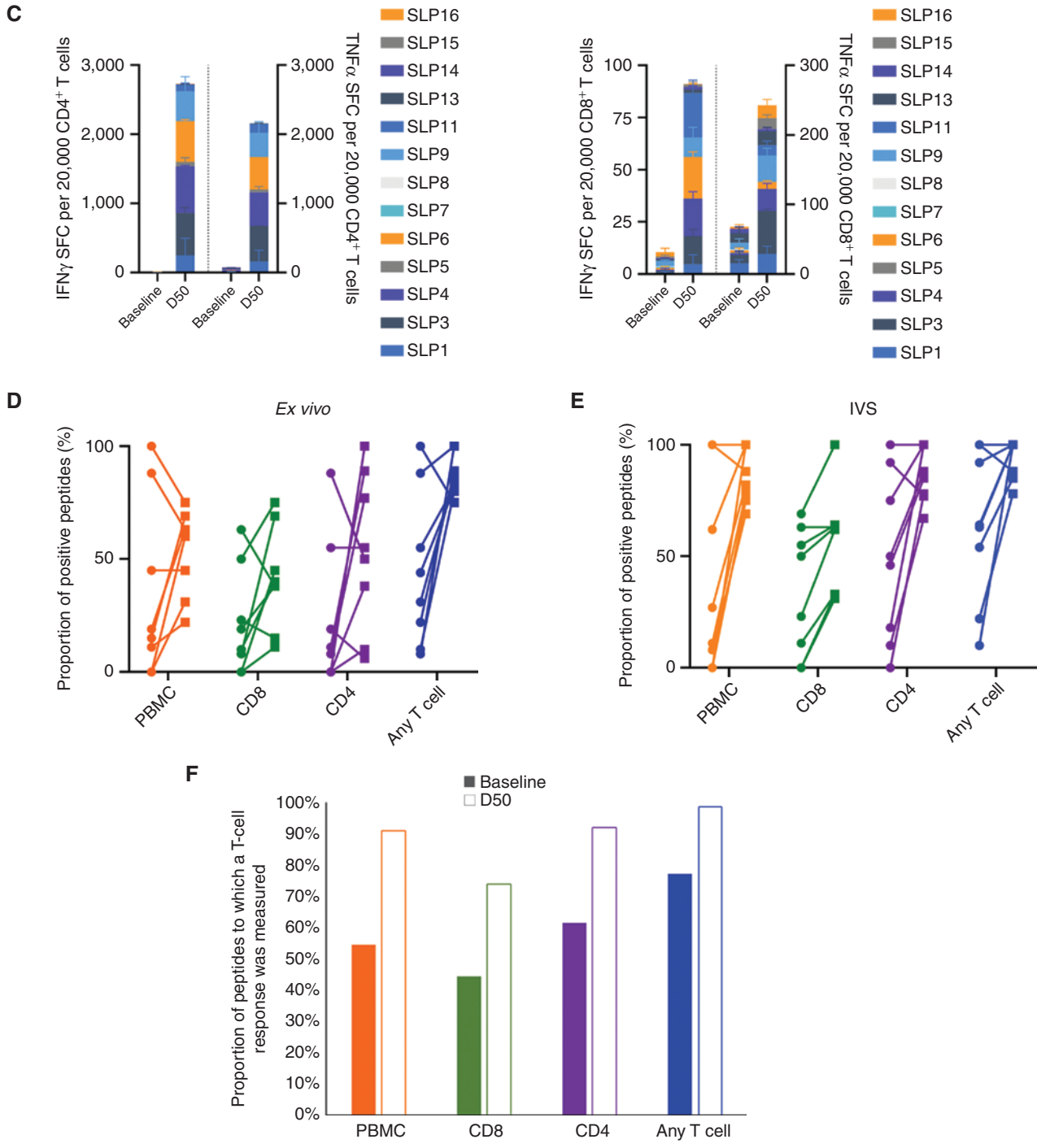

Figure 4. ***(Continued)*** **C,** For the IVS fluorospot assay, PBMCs were expanded for 10 days with OLPs spanning SLPs represented in each pool. On day 10, expanded cells were tested in an IFNγ/TNFα fluorospot assay and stimulated with each individual peptide. Data are reported as the mean SFC per 20,000 $CD4^+$ or $CD8^+$ T cells, also broken out by pools. **D** and **E,** The proportion of peptides positive by the DFR(eq) test with a *P* value of ≤0.05 (21) is shown for the *ex vivo* (**D**) and IVS (**E**) fluorospot assays. Circles represent baseline, squares represent D50 timepoint, and each line represents one vaccinated subject (53). **F,** Proportion of positive peptides using either *ex vivo* or IVS fluorospot assay.

(Supplementary Table S7). The TNFα results were similar, but with slightly lower medians. Overall, these data show that empirical selection of stimulatory neoantigens with ATLAS results in a greater proportion of immunogenic responses after vaccination than previously reported (8, 9).

DISCUSSION

Finding therapeutic T-cell targets has been critical to progress against cancer. The identification of relevant tumor-specific neoantigens holds the promise of improving

cancer immunotherapy through broad expansion of tumor-expressed and immunogenic targets, but determination of which mutations are relevant for an individual patient has been elusive. Although *de novo* neoantigen-specific vaccine responses may be important for successful immunotherapy (22), *in silico* neoantigen selection has yielded poor predictive value and provides little confidence that putative prioritized antigens are relevant to the individual patient's HLA type and T-cell repertoire. Moreover, the success of tumor-infiltrating lymphocyte (TIL) therapies shows that preexisting T cells can be protective if they are successfully expanded and otherwise augmented (reviewed in ref. 23). *De novo* responses may also carry additional risk of off-tumor toxicity as the T cells generated are novel to the patient. Here, we describe the implementation of an empirical method to identify immunogenic tumor mutations using a biological assay customized for the patient. ATLAS comprehensively screens all tumor-specific mutations and identifies personalized neoantigens to which a patient's T cells have already responded (i.e., preexisting T-cell responses). Importantly, to be detected by the ATLAS bioassay, identified neoantigens must have been effectively processed and presented in the context of the patient's tumor for recall T-cell responses to be generated. The ATLAS assay has successfully identified protective infectious disease antigens for use in candidate vaccines and immunotherapies (24–27). The ATLAS assay is also well suited for high-throughput and comprehensive screening of all somatic mutations in the setting of solid-tumor cancers because ATLAS is HLA-agnostic and inclusive of all genetic and ethnic backgrounds and does not rely on epitope predictions. In addition, ATLAS identifies whether the T-cell response a patient generated to each of their neoantigens is potentially beneficial (stimulatory) or deleterious (inhibitory).

In the retrospective research cohort of nine patients with lung cancer, screening of peripheral blood T cells against respective tumor mutanomes revealed that approximately 10% of mutations were immunogenic (both $CD4^+$ and $CD8^+$ T-cell subsets), and, of these, 6% were newly discovered Inhibigens. The relative proportion of neoantigens was highly variable between subjects, confirming previous reports (28). By contrast, the observed proportions of neoantigens greatly exceed the neoantigen-specific response frequencies of 1% to 2% identified in TIL from tandem minigenes or in peripheral blood screens of PD-1–sorted T cells. This discrepancy could be due to multiple factors. First, ATLAS libraries are built based on nonsynonymous mutations (relative to germline) identified in DNA, whereas many other screens have filtered out mutations based on RNA expression prior to *in silico* selection (29). Our data suggest that this approach may remove some bona fide neoantigens, as these analyses only measure RNA expression in the region of tumor biopsied and do not account for tumor heterogeneity. Conversely, it is possible that our screens identify neoantigens that were expressed in the tumor in the past but have since been immunoedited. Next, TIL approaches require sufficient tumor material to facilitate T-cell outgrowth from resected tumor fragments. It is possible that not all neoantigen-specific T cells will migrate out of the tumor and expand during this process, thereby resulting in a perceived lower response breadth. Indeed, a recent publication showed that addition of 4-1BB agonistic antibody to tumor explants resulted in a greater proportion of neoantigen-specific T-cell responses emerging from tumors (30). Third, multimer approaches are limited in allele coverage and are dependent on algorithmic predictions for selection (31). Finally, peptide-based approaches require epitope prediction and exogenous loading of MHC class I or class II epitopes for presentation, whereas the ATLAS approach utilizes native intracellular antigen processing and presentation.

For each of the datasets presented here, when neoantigens identified by ATLAS were compared with predicted epitopes based on NetMHCpan algorithms (17, 32), there was minimal overlap. In the retrospective lung cancer cohort, for example, the MHC I prediction algorithm had a 13% positive predictive value relative to ATLAS outputs. When the algorithm predicted an antigen that was confirmed by ATLAS, approximately half of the time the response was identified as inhibitory, a biological response that cannot currently be predicted by an algorithm. In addition, 32% of the neoantigens identified by ATLAS were not *in silico* predicted. NetMHCIIpan was even less accurate for MHC II where the algorithm had a 3% positive predictive value (all were characterized by ATLAS as Inhibigens) and a 93% false negative rate. The poor predictive value of epitope prediction algorithms based on affinity is not surprising; indeed, van Rooij and colleagues (33) showed that less than 1% of predicted high-affinity binders from a patient with melanoma were recognized by the patient's T cells. Moreover, a mass spectrometry approach recently revealed that weakly binding neoepitopes could be protective tumor antigens in mouse models (34), confirming that vaccines designed based upon predicted high-affinity binding epitopes may miss many appropriate antigens and include potentially unsuitable targets. In addition, in order to prioritize predicted epitopes for vaccination using algorithms, supplementary selection criteria are commonly used, such as selecting mutations in known cancer genes or those that generate novel sequences such as insertions or deletions, or using criteria such as expression levels, DNA copy number, or DAI (reviewed in ref. 35). In the current study, no enrichment for neoantigens or Inhibigens was observed by these criteria. There was a slight trend for increased RNA expression of neoantigens, but the differences were small with a large overlap in distributions. We acknowledge that only one prediction algorithm was used in this study, and there are others available for public or private use that may yield different outcomes. In addition, multiple groups are trying to improve on existing algorithms by using mass spectrometry and monoallelic cell line approaches (34, 36, 37). Despite progress in the various *in silico* approaches, our data suggest that the heterogeneity of MHC, the complex biology of antigen processing, presentation, T-cell responsiveness, and the context in which T cells are educated to mutations during cancer initiation and progression are far more complex than can be currently modeled *in silico*.

The complexity of neoantigen identification is exemplified by the detection of Inhibigens in our study. In ATLAS, these responses are characterized by the reduction of IFNγ and/or TNFα secretion to levels that are statistically below baseline controls. As Inhibigen responses have also been found in screens of nonmutated tumor antigens and pathogen proteins (38, 39), these responses do not appear to be unique

to cancer mutations. The biological relevance of Inhibigen-specific responses was demonstrated in the B16F10 melanoma model, where inclusion of ATLAS-defined Inhibigen peptides to an otherwise protective vaccine abrogated efficacy and, in some cases, accelerated tumor progression. Corresponding loss of neoantigen-specific T-cell immunogenicity to protective antigens was observed, as well as reduced tumor infiltration by $CD8^+$ T cells, macrophages, and dendritic cells. Vaccine-augmented tumor growth, rather than protection, has been reported in other mouse models and attributed to tolerization of antitumor response (40, 41).

Further investigation is required to reveal how ATLAS-identified Inhibigens exert protumor effects and determine whether the phenotype is a property of the Inhibigen itself, or whether T cells are aberrantly educated to Inhibigens in the context of the tumor. Several possibilities exist: (i) Inhibigen-specific Tregs may be suppressing antitumor immune responses. Tregs are functionally and phenotypically heterogeneous and can act through a number of mechanisms, including production of inhibitory cytokines, cytolysis, metabolic disruption of effector T cells, and/or inhibition of dendritic cell maturation and function (42). Although the broader class of Tregs cannot be fully discounted at this time, simple induction of classic Tregs ($CD4^+CD25^+FOXP3^+$) is unlikely, as these Tregs were not more abundant in the TME of Inhibigen-immunized mice relative to controls. Moreover, with ATLAS, Inhibigens are commonly identified in the $CD8^+$ T-cell subset. (ii) Inhibigens might modulate myeloid-derived cells directly, either by disrupting antigen presentation or by inducing these cells to express immunosuppressive molecules such as indoleamine 2,3-dioxygenase that suppress effector T-cell function (43). Monocyte-derived suppressor cells (MDSC) are also capable of suppressing effector T-cell responses; however, Inhibigens are identified in ATLAS in the context of a defined culture containing uniform monocyte-derived dendritic cells (MDDC) and sorted T cells during a brief overnight exposure. The differentiation of MDDCs to MDSCs in this short time frame is unlikely. (iii) Effector T cells responding to Inhibigens could be driven into a suppressive state. T-cell dysfunction due to persistent antigen stimulation of the T-cell receptor (TCR) is a common feature of cancer, and it is possible that Inhibigens induce tolerance through this mechanism (44). However, it is unclear how T-cell dysfunction of an Inhibigen-specific cell could suppress effector T cells against other antitumor antigens *in trans*. Alternatively, regulation of downstream TCR signaling through inhibition of protein kinase or phosphatase activity has been shown to disrupt T-cell activation (45), and Inhibigens could regulate these pathways.

To distinguish between these possibilities or uncover novel mechanisms of inhibition, future studies will explore the presence of inhibitory cytokines (e.g., IL10, TGFβ, and IL35) in various cell subsets after *in vitro* and *in vivo* exposure to Inhibigens. In addition, it will be critical to map the $MMP9_{FS}$ minimal inhibitory epitope, which will enable tetramer development and characterization of cytokine profiles and transcriptomic patterns of purified Inhibigen-specific T cells. Inhibigen identification and characterization in additional syngeneic mouse tumor models will also be explored; however, the frequent identification of Inhibigens in many human screens underscores their broad relevance. We propose that T cells responding to Inhibigens, or the antigen-presenting cells (APC) that display them, can affect the local and systemic immune environment, leading to local changes in the TME as well as tumor growth kinetics; this accentuates the importance of utilizing *ex vivo* assays to define and exclude such antigens from any personalized cancer vaccine or cell therapy.

GEN-009 is a personalized cancer vaccine that includes only ATLAS-identified neoantigens and excludes Inhibigens. Analysis of the initial cohort of enrolled patients in our phase I clinical trial (NCT03633110) showed that generation of GEN-009 vaccine was consistently feasible and well tolerated. All vaccinated patients had detectable T-cell immune responses to the neoantigens in their vaccine, including immune responses overall against 99% of all immunized peptides, which is a remarkable and unprecedented result in the field (8, 9, 46). Broad $CD4^+$ and $CD8^+$ T-cell responses across multiple neoantigens were generated, including $CD8^+$ T-cell responses that were measurable directly *ex vivo*. Both outcomes are notable in comparison with previously reported first-in-human, *in silico*–selected neoantigen vaccines (8, 9) in which *ex vivo* $CD8^+$ T-cell responses were undetectable, and the proportion of peptides to which responses were measured was approximately 60% after IVS. These prior neoantigen vaccine studies could neither identify nor exclude Inhibigens with their *in silico* approaches. Notably, if Inhibigens were included in a cancer vaccine, they would likely appear as undetectable in an IFNγ ELISpot analysis. The GEN-009-101 study continues to evaluate the GEN-009 vaccine, excluding Inhibigens, in combination with standard-of-care immunotherapy regimens.

In summary, the translational and clinical data presented here demonstrate the feasibility of a high-throughput personalized approach to identifying mutation-associated neoantigens in murine models and patients with cancer. Administration of a vaccine optimized via selection of neoantigens with ATLAS should amplify preexisting immunity, create *de novo* responses to the same neoantigens, and allow expansion of targets via epitope spread. The ATLAS approach has unique advantages as it identifies both stimulatory and novel inhibitory antigens (Inhibigens). We hypothesize that the proportion of Inhibigen- to neoantigen-specific T-cell responses may correlate with clinical prognosis and are currently exploring this in a prospective study. It is possible that these inhibitory T-cell responses are associated with observations of resistance or hyperprogression in some subjects treated with ICI (reviewed in ref. 47); however, our data do not support dysregulation of $PD\text{-}1^+$ Tregs as was recently reported (48). If the deleterious impact of Inhibigens by therapeutic vaccination in a mouse model translates to humans, then it is crucial to identify and exclude these Inhibigens from cancer immunotherapies. In support of this empirical antigen selection approach, a preplanned interim analysis of the first cohort of patients enrolled in the GEN-009-101 clinical trial confirmed that the stimulatory antigens identified via ATLAS were bona fide immunogenic neoantigens. Overall, Genocea's ATLAS platform provides critical information about a patient's individual neoantigen immunity and could enable cancer immunotherapies that augment a patient's preexisting antitumor response and improve clinical outcomes.

METHODS

Study Design

The objectives of these studies were to explore the peripheral T-cell responses to tumor mutations in human subjects and in mouse models. Our hypothesis was that unbiased measurement of T-cell responses to each mutation in a subject's tumor would yield more accurate and biologically relevant information about neoantigen specificities than the *in silico* methods commonly used for neoantigen prediction. To this end, we recruited patients with cancer for an observational study, explored the phenotype of inhibitory and stimulatory T-cell responses in a mouse model, and finally began a phase I/IIa clinical trial to treat patients with cancer with the GEN-009 immunotherapy. Power calculations were performed for group sizes in the mouse model.

ATLAS Process

The ATLAS assay has been used extensively for screening of T-cell responses in human subjects, with detailed methods described previously (12, 24, 25, 27, 49, 50).

Identification of Tumor-Specific Mutations. Genomic DNA from formalin-fixed, paraffin-embedded (FFPE) tumor sections and matched saliva was isolated and subjected to whole-exome capture and paired-end sequencing and RNA-seq using the Nova-seq platform. Sequencing and data analysis were performed at Personalis, which have demonstrated accuracy and precision of their experimental protocols, with a sensitivity of 99% for SNVs (3% false positive rate) and 94% for indels (3% false positive rate). The coverage was 150× for normal and 300× for tumor. Somatic variants were called from the exome reads and reference human genome using hs37d5 and BWA and STAR alignment tools, and variants were called using MuTect, Verdict, and Fusion Catcher. Genomic DNA extracted from B16F10 tumors raised in C57BL/6 mice was sequenced using whole-exome sequencing with HiSeq2500 platform. One hundred base pair (bp) paired-end sequencing was performed at Otogenetics, and sequences were aligned against the mm10 reference genome. The coverage was 120×. The B16F10 tumor was then compared against germline C57BL/6 DNA from mouse tail to identify tumor-specific mutations using Strelka and Verdicts. The original B16F10 cell line (ATCC, passage 6) was also sequenced to confirm presence of these same mutations. Variant annotation was performed using SnpEff (dataset: National Center for Biotechnology Information Sequence Read Archive accession #PRJNA662658).

Discovery of Neoantigens. For the lung cohort and murine model studies, 399-bp DNA fragments encoding each of the identified mutations were synthesized (GENEWIZ or Twist Biosciences) and cloned into a proprietary plasmid (pGEN4) with each fragment ligated in-frame with a DNA sequence encoding the SIINFEKL epitope from chicken ovalbumin. In the GEN-009-001 study, 123-bp DNA fragments encoding each identified mutation were synthesized (GENEWIZ) and cloned into a proprietary vector (pGEN132) containing a red fluorescent protein (Fresno RFP, ATUM Bio) coding sequence in-frame. Clones expressing the first 399 or 123 bp (depending on use of pGEN4 or pGEN132, respectively) of green fluorescent protein from *Branchiostoma lanceolatum* (blFP-Y3; abbreviated NG) were used as an irrelevant negative control antigen. Sequence-verified clones were transformed into *E. coli* containing a separate plasmid encoding a cytoplasmic variant of listeriolysin O (cLLO) for screening of $CD8^+$ T cells or lacking cLLO for $CD4^+$ T cells (13). Expression was induced using IPTG and verified either by Western blot or by detection of RFP fluorescence. Clones and negative controls were fixed with formalin, washed, normalized, and then randomly rearrayed in duplicate in 384-well plates. Plates were stored at −80°C until used (13).

PBMC samples were collected by either venipuncture or apheresis, enriched via density gradient centrifugation, and viably frozen within 8 hours. Frozen PBMCs were thawed and sorted using microbeads (Miltenyi) to enrich for monocytes and to separate the $CD4^+$ and $CD8^+$ T cells. The monocytes were cultured with recombinant human GM-CSF and recombinant human IL4 for 7 days to differentiate into MDDCs. The $CD4^+$ and $CD8^+$ T cells were separately expanded nonspecifically for 1 week using anti-CD3 and anti-CD28 microbeads (Invitrogen) and low-dose IL2. Due to cell limitations, not all mutations could be screened against both T-cell subsets for all patients. Under those circumstances, $CD8^+$ T cells were prioritized.

For screening of ATLAS libraries, autologous MDDCs were added to individual wells of the arrayed *E. coli* plates, with a target of 5,000 cells per well. Plates were incubated at 37°C with 5% CO_2 for 2 hours to facilitate antigen uptake and processing. After washing, 80,000 autologous T cells (either $CD4^+$ or $CD8^+$) were added to each well and incubated overnight. In addition to the negative controls expressing blFP-Y3 (NG), phorbol 12-myristate 13-acetate (PMA)/ionomycin mitogen (81 nmol/L and 1.34 μmol/L, respectively) was added as a positive control for T-cell activity. Supernatants were transferred to new 384-well plates and frozen at −20°C until analyzed for IFNγ and TNFα cytokine levels by Meso Scale Discovery (MSD) assay. Briefly, supernatants and calibrators were added to precoated MSD plates and incubated. After washing, the SULFO-TAG–conjugated detection antibody was added, and after washing, read buffer was added followed by analysis with an MSD instrument.

The murine neoantigen screens were performed as described above, with the exception that only $CD8^+$ splenocytes were tested, and the RAW309 Cr.1 macrophage cell line (ATCC TIB-69) was used as APC. The RAW309 cells were incubated overnight and then the ATLAS library was added the next day. The original ATLAS screen interrogated the entire mutanome, and two repeat screens evaluated a subset of 174 clones based on the initial data.

Responses were identified based on mean and SD estimates from cytokine levels of both the negative control (NG) and replicate test wells from MSD plates based on defined standards. Data from MSD plates are first log-transformed (natural log) prior to analysis. Any test wells with responses that do not fall within the linear range of the standard curve are excluded. Given the approximate normal distribution of the data, a span of 2 SDs from the mean represents a 95% confidence interval for nonresponse. Therefore, a threshold of 2 SDs above the mean was used for identification of neoantigens with the expectation of a false positive rate of 5%. Z-transformed data based on calculated mean and SDs were used to identify and visualize antigen calling from MSD plate data.

Cell Lines

B16F10 cells were obtained from the ATCC, expanded to six passages, and frozen as a stock for use across mouse studies. Thawed cells were cultured for up to 4 days without passaging prior to mouse injection. Cells at final passage prior to freezing tested negative for *Mycoplasma* by Lonza MycoAlert detection kit (2018) and negative for all infectious disease by Charles River Research Animal Diagnostic Services (2018). Whole-exome sequencing of the final frozen stock was performed by Otogenetics confirming cell line identity (2018).

Mice

Female 6- to 8-week-old C57BL/6 mice were obtained from The Jackson Laboratory for use in mouse studies under the Institutional Animal Care and Use Committee–approved protocol #18-0625-1: Evaluation of the effects of vaccination in mouse tumor models.

Murine Tumor Models

SLPs (27 aa) were synthesized by GenScript, New England Peptide, or 21st Century Biochemicals. B16F10 melanoma cells (1×10^5;

ATCC CRL-6475) were inoculated subcutaneously into the flanks of 6- to 8-week-old female C57BL/6 mice. Tumor-bearing mice were randomized and then injected s.c. in the tail base on days 3, 10, and 17 with formulations containing 50 μg per SLP, 5 μg CpG ODN1826 (Invivogen), 5 μg 3D-PHAD (Avanti), and 25 μg QS21 (Invivogen). Tumor sizes were measured every 3 days until ≥2,000 mm^3 and daily until tumor ≥2,500 mm^3, upon which mice were euthanized. For immunogenicity studies, mice were immunized on days 0 and 7 in the absence of tumor and euthanized for splenocyte analysis on day 14.

ELISpot assay for the measurement of IFNγ from mouse T cells pulsed with antigen has been previously described (51, 52). Stimulants of media alone, PMA/ionomycin (200 ng/mL; 1 μg/mL), or OLPs (15 mer overlapping by 11 aa; 1 μg/peptide) were prepared. Stimulants and cells were coincubated for 16 hours at 37°C after which IFNγ secretion was detected using anti-IFNγ capture antibody (10 μg/mL clone AN18; Mabtech) and anti–IFNγ-biotin (1 μg/mL clone R4-6A2; Mabtech). All SFCs were normalized to 1×10^6 splenocytes.

TILs were isolated using enzymatic digestion with collagenase I (100 U/mL; Worthington), collagenase IV (500 U/mL; Sigma), and DNAse (200 μg/mL; Sigma). After digestion, single-cell suspensions were filtered through a 70-μm filter, and lymphocytes were sorted using CD45 microbeads (Biolegend, Clone 30F11, STEMCELL isolation kit). Cells were stained in 5% FBS in PBS. Antibodies included fixable viability dye (BD), CD19 (6D5, Biolegend), NK1.1 (PK136, Biolegend), CD4 (RM4-5, Thermo Fisher Scientific), CD8 (53-6.7, Biolegend), CD25 (PC61, Biolegend), CD3 (17A2, Biolegend), and CD45 (30-F11, Biolegend). Collection was performed on a BD LSRFortessa, and analysis was performed using FlowJo.

IHC

For IHC, resected and FFPE tumors were prepared and sectioned by JMD Histology and Histologistics. Slides were deparaffinized and subjected to antigen retrieval in either citrate or EDTA buffer at 100°C for 20 minutes in a TintoRetriever pressure cooker from Bio SB. Slides were blocked with 10% goat serum and incubated with primary antibody overnight at 4°C. Antibodies included CD4 (D7D2Z, 1:50), CD8 (D4W2Z, 1:200), FoxP3 (D6O8R, 1:100), F4/80 (D2S9R, 1:200), and CD11c (D1V9Y, 1:350) from Cell Signaling Technology. All washes were performed with TBS-Tween20. Slides were incubated with polink-1 AP rabbit secondary antibody and subsequently with permanent red chromogen dye from Origene. Tissues were counterstained with hematoxylin and mounted with aqueous mounting medium. Images were acquired on the EVOS FL Auto imaging system (Life Technologies) and prepared in ImageJ (NIH) software.

Vaccine Manufacture

ATLAS-prioritized neoantigens were manufactured as SLPs (27 aa) under cGMP conditions, formulated in physiologic buffer, and frozen at −20°C. Each personalized vaccine consisted of between 4 and 20 SLPs divided into 4 pools, with each pool containing 1 to 5 SLPs. The specific number of SLPs in each patient's vaccine was dependent on the number of neoantigens identified by ATLAS and the number that could be synthesized and formulated. Peptides were combined with poly-ICLC (Hiltonol) for subcutaneous administration.

Clinical Study Design

GEN-009-101 is a first-in-human study evaluating the safety, immunogenicity, and anticancer activity of the GEN-009 vaccine in patients with solid tumor malignancies. The clinical trial was registered with designation NCT03633110 (https://clinicaltrials.gov/ct2/show/NCT03633110). Part A, for which we now report preliminary results, enrolled patients without evidence of disease after initial therapy. The primary endpoint is safety and immunogenicity of administered peptides. The vaccine was injected s.c. for 5 doses over 6 months on days 1, 22, 43, 85, and 169 (Supplementary Fig. S9). The clinical sites enrolling the study obtained written informed consent from patients via an Institutional Review Board–approved consent form, and the trial was conducted in accordance with recognized ethical guidelines under the supervision of an institutional or central review board.

Patients

Part A was open to adults with cutaneous melanoma, NSCLC, squamous cell carcinoma of the head and neck, or urothelial carcinoma, who had completed standard treatment (e.g., surgical resection, adjuvant therapy, and/or radiotherapy) with curative intent. Additional eligibility requirements included Eastern Cooperative Oncology Group (ECOG) performance status of 0 or 1 and adequate hematologic, liver, and kidney function. Exclusion criteria included active autoimmune disease, primary immune deficiency, or immunosuppressive therapies within 28 days prior to study.

Procedures and Treatment

All patients signed written informed consent after the nature and possible consequences of the studies were explained, and before the conduct of any protocol-specific procedures. Leukapheresis was performed at baseline and day 50 for the ATLAS process and immunogenicity assessments. In addition, whole blood was collected at additional timepoints for immunogenicity. Disease assessment, CT, or MRI was performed within 4 weeks prior to GEN-009 dosing to rule out disease recurrence. Patients with urothelial carcinoma who did not have a complete cystectomy additionally underwent urine cytology and, if appropriate, cystoscopy to verify disease status.

Disease-free survival is being assessed every 12 weeks through the first year of treatment, and every 26 weeks thereafter. Safety measurements performed throughout the vaccine treatment period included evaluation of adverse events, clinical laboratory tests, physical examination, vital signs, and ECOG status. Adverse events are graded according to the NCI Common Terminology Criteria for Adverse Events v5.0.

Cellular Immune Responses to Vaccination

In Vitro *Stimulation of PBMCs.* PBMCs were stimulated in a 24-well plate at 5×10^6 cells/well with 1 μg each peptide/mL in the presence of IL7. On days 3, 6, and 9, IL2 was added. After 10 days, T cells were sorted for $CD4^+$ or $CD8^+$ T cells using magnetic bead isolation (Miltenyi) before plating for the fluorospot assay.

Fluorospot Assays. 96-well precoated human IFNγ/GrB (*ex vivo*) or IFNγ/TNFα (IVS) fluorospot kits (Mabtech) were used. OLPs (15 mer overlapping by 11 aa) were synthesized for all vaccinated SLPs. For the *ex vivo* fluorospot, 2×10^5 PBMC or 2×10^5 CD4- or CD8-depleted PBMCs were added to each well with 1 μg/mL each OLP and incubated for 48 hours. For the IVS fluorospot, 2×10^4 $CD4^+$ or $CD8^+$ T cells, 5×10^3 lymphocyte-depleted PBMCs, and 1 μg/mL each OLP were added and incubated for 24 hours. Plates were washed and then detection antibody was added, followed by anti–BAM-490 and SA-550 (Mabtech). After washing, fluorescence enhancer was added, and then the plates were read on the AID iSpot Reader System (AID).

Statistical Analysis

ATLAS Screens. After bias correction and failure removal, the amount of cytokine production per well was normalized to the multiple redundant measurements of the negative control neon green (NG). Only cytokine measurements that fell within the linear range of the standard curves run on the same plate were included

in analyses. A candidate antigen was defined as stimulatory or inhibitory if the cytokine production was 2 times the median average deviations above or below the median of the negative controls, respectively.

Murine ATLAS Screen. In addition to B16F10 ATLAS clones, clones expressing mouse actin, a housekeeping gene for which mice should not have any T-cell reactivity, were included as negative control antigen arrayed randomly across the plates. For each MSD screening plate and cytokine, a multilevel model was fit to the log-transformed data. The estimated mean response to the negative control was subtracted from the mean response to each candidate neoantigen, and the estimated residual SD was divided by this difference to yield a normalized log cytokine concentration that can be interpreted as SDs above or below the background control. Values greater than 2 were deemed stimulatory responses, and values less than −2 were deemed inhibitory responses.

GEN-009 Fluorospot Assays. A response was defined as positive if the mean SFC exceeded the LOD and if the *P* value between the test and negative control was ≤ 0.05 by the DFR(eq) test (53).

Authors' Disclosures

H. Lam reports a patent for PCT/US18/23442 pending. L.K. McNeil reports patents for PCT/US18/23442 and PCT/US20/33277 pending to Genocea Biosciences. R.B. Cohen reports grants and personal fees from Genocea Biosciences during the conduct of the study; and grants and personal fees from HEAT Biologics outside the submitted work. M.L. Johnson reports grants from Genocea Biosciences during the conduct of the study; and personal fees from Otsuka and Astellas Pharma, grants and other from Genentech/Roche, Boehringer Ingelheim, AstraZeneca, Calithera Biosciences, Merck, Loxo, Sanofi, Mirati Therapeutics, Pfizer, Guardant Health, Incyte, AbbVie, Atreca, GlaxoSmithKline, Gritstone Oncology, Janssen, Lilly, Novartis, Amgen, Daiichi Sankyo, EMD Serono, and WindMIL, other from Ribon Therapeutics, Achillies Therapeutics, Association of Community Cancer Centers, Bristol-Myers Squibb, and G1 Therapeutics, and grants from Kadmon, Genmab, Stem CentRx, Checkpoint Therapeutics, Array BioPharma, Regeneron, Hengrui Pharmaceuticals, Lycera, BeiGene, Tarveda Therapeutics, CytomX Therapeutics, Dynavax, Corvus Pharmaceuticals, Genocea Biosciences, Adaptimmune, Syndax, Neovia Oncology, Acerta Pharma, Takeda, Shattuck Labs, Apexigen, Atreca, OncoMed, Immunocore, Jounce Therapeutics, University of Michigan, TCR2 Therapeutics, Arcus Biosciences, Ribon Therapeutics, BerGenBio, Tmunity Therapeutics, and Seven and Eight Biopharmaceuticals outside the submitted work. M.L. Gillison reports other from Genocea Biosciences during the conduct of the study; and personal fees from Gilead, EMD Serono, BMS, Kura, Shattuck Labs, Bayer Healthcare, Roche, BioNTech AG, Merck, and NewLink Corporation and other from BMS, Kura, and Bicara Therapeutics outside the submitted work. M.N. Stein reports grants from Genocea Biosciences during the conduct of the study; and grants from Exelixis, Tmunity, Seattle Genetics, Nektar, Lilly, Bristol Myers Squibb, Harpoon, and Janssen Oncology outside the submitted work. U.N. Vaishampayan reports grants and personal fees from BMS, Inc., and Alkermes, and personal fees from Exelixis, Bayer, Pfizer, Merck, and Onc Live outside the submitted work. A.P. DeCillis reports personal fees from Genocea Biosciences, Exelixis, Osmol, Cybrexa, Codiak, Monopteros, Pyramid, and Evelo outside the submitted work. J.J. Foti reports other from Genocea Biosciences during the conduct of the study. W. Broom reports a patent for PCT/US18/23442 pending; in addition, W. Broom was an employee of Genocea Biosciences at the time of his contribution to this article. E.M. Jaffee reports personal fees from Genocea Biosciences during the conduct of the study; and personal fees from CSTONE, Achilles, Adaptive Biotech, dragonfly, and Parker Institute, grants from Lustgarten Foundation outside the submitted work. K.-K Wong is a founder and equity holder of G1 Therapeutics and has consulting and sponsored research with AstraZeneca, Janssen, Pfizer/Array Biopharma, Novartis, Merck, Zentalis, and Genocea Biosciences as well as sponsored research (only) with Takeda, BMS, Mirati, Alkermes, Merus, Amgen, Ansun Biopharma, Eliven Therapeutics, Tvardi Therapeutics, Delfi Diagnostics, and Dracen Pharmaceuticals. C.G. Drake reports other from Genocea Biosciences during the conduct of the study; and other from Bayer, BMS, Compugen, F-Star, Kleo, Merck, Merck-Serono, Pfizer, Roche/Genentech, Shattuck Labs, Tizona, and Werewolf outside the submitted work; in addition, C.G. Drake had a patent for LAG-3 issued and licensed to BMS. P.M. Carroll reports a patent for PCT/US18/23442 pending. T.A. Davis reports personal fees and other from Genocea Biotherapeutics during the conduct of the study; and personal fees and other from Genocea Biosciences outside the submitted work. J.B. Flechtner reports personal fees and other from Genocea Biosciences outside the submitted work; in addition, J.B. Flechtner had patents for PCT/US18/23442 and PCT/US20/033277 pending to Genocea Biosciences. No disclosures were reported by the other authors.

Authors' Contributions

H. Lam: Conceptualization, data curation, formal analysis, supervision, validation, investigation, visualization, methodology, writing–original draft, writing–review and editing. **L.K. McNeil:** Formal analysis, supervision, investigation, methodology, writing–original draft, writing–review and editing. **H. Starobinets:** Conceptualization, resources, data curation, formal analysis, investigation, visualization, methodology, writing–review and editing. **V.L. DeVault:** Conceptualization, resources, data curation, formal analysis, validation, investigation, visualization, methodology, writing–review and editing. **R.B. Cohen:** Resources, investigation. **P. Twardowski:** Resources, investigation. **M.L. Johnson:** Resources, investigation. **M.L. Gillison:** Resources, investigation. **M.N. Stein:** Resources, investigation. **U.N. Vaishampayan:** Resources, investigation. **A.P. DeCillis:** Conceptualization, resources, investigation. **J.J. Foti:** Resources, investigation, methodology. **V. Vemulapalli:** Resources, data curation, software, formal analysis, validation, visualization, methodology. **E. Tjon:** Resources, data curation, software, formal analysis, validation, visualization, methodology. **K. Ferber:** Resources, data curation, software, formal analysis, validation, visualization, methodology. **D.B. DeOliveira:** Resources, investigation, methodology. **W. Broom:** Resources, formal analysis, supervision, investigation. **P. Agnihotri:** Investigation, methodology. **E.M. Jaffee:** Conceptualization. **K.-K. Wong:** Conceptualization. **C.G. Drake:** Conceptualization. **P.M. Carroll:** Conceptualization. **T.A. Davis:** Conceptualization, resources, supervision, validation, investigation, methodology, writing–review and editing. **J.B. Flechtner:** Conceptualization, resources, data curation, formal analysis, supervision, validation, investigation, visualization, methodology, writing–original draft, writing–review and editing.

Acknowledgments

The authors are grateful to the patients who consented to participate in our observational study and clinical trial. They also thank Genocea's extraordinary clinical operations team (Jessica Price, Kevin Mancini, and Rich Hernandez) and manufacturing team including Narinderjeet Singh and Manish Jain. They also thank the ATLAS team including Louisa Dowal, Tulin Dadali, Crystal Cabral, Michael O'Keeffe, Christopher Warren, James Loizeaux, Mariya Croll, James Perry, Anna Lyubetskaya, Erick Donis, and Matthew Lanchantin; the Translational Immunology team including Mara Shainheit, Tyler Fenske, Megan Croshier, Devin Champagne, Gabriella Santone, and Syukri Shukor; the Computational Biology team including Ning Wu

and Huilei Xu; and the Preclinical Development team including Stephanie Rinaldi, Sanmit Adhikari, Osaruese Odeh, Peri Matatia, Simran Singh, Dylan Sheehan, and Cindy Nguyen.

Received April 15, 2020; revised September 15, 2020; accepted November 13, 2020; published first January 27, 2021.

REFERENCES

1. Sharma P, Allison JP. The future of immune checkpoint therapy. Science 2015;348:56–61.
2. Gubin MM, Zhang X, Schuster H, Caron E, Ward JP, Noguchi T, et al. Checkpoint blockade cancer immunotherapy targets tumour-specific mutant antigens. Nature 2014;515:577–81.
3. Riaz N, Havel JJ, Makarov V, Desrichard A, Urba WJ, Sims JS, et al. Tumor and microenvironment evolution during immunotherapy with nivolumab. Cell 2017;171:934–49.
4. McGranahan N, Furness AJ, Rosenthal R, Ramskov S, Lyngaa R, Saini SK, et al. Clonal neoantigens elicit T cell immunoreactivity and sensitivity to immune checkpoint blockade. Science 2016;351:1463–9.
5. Kreiter S, Vormehr M, van de Roemer N, Diken M, Lower M, Diekmann J, et al. Mutant MHC class II epitopes drive therapeutic immune responses to cancer. Nature 2015;520:692–6.
6. Alspach E, Lussier DM, Miceli AP, Kizhvatov I, DuPage M, Luoma AM, et al. MHC-II neoantigens shape tumour immunity and response to immunotherapy. Nature 2019;574:696–701.
7. Feau S, Garcia Z, Arens R, Yagita H, Borst J, Schoenberger SP. The CD4(+) T-cell help signal is transmitted from APC to CD8(+) T-cells via CD27-CD70 interactions. Nat Commun 2012;3:948.
8. Ott PA, Hu Z, Keskin DB, Shukla SA, Sun J, Bozym DJ, et al. An immunogenic personal neoantigen vaccine for patients with melanoma. Nature 2017;547:217–21.
9. Sahin U, Derhovanessian E, Miller M, Kloke BP, Simon P, Lower M, et al. Personalized RNA mutanome vaccines mobilize poly-specific therapeutic immunity against cancer. Nature 2017;547:222–6.
10. Linette GP, Carreno BM. Neoantigen vaccines pass the immunogenicity test. Trends Mol Med 2017;23:869–71.
11. Jensen KK, Andreatta M, Marcatili P, Buus S, Greenbaum JA, Yan Z, et al. Improved methods for predicting peptide binding affinity to MHC class II molecules. Immunology 2018;154:394–406.
12. Nogueira C, Kaufmann JK, Lam H, Flechtner JB. Improving cancer immunotherapies through empirical neoantigen selection. Trends Cancer 2018;4:97–100.
13. Higgins DE, Shastri N, Portnoy DA. Delivery of protein to the cytosol of macrophages using Escherichia coli K-12. Mol Microbiol 1999;31:1631–41.
14. Van Wagoner N, Fife K, Leone PA, Bernstein DI, Warren T, Panther L, et al. Effects of different doses of GEN-003, a therapeutic vaccine for genital herpes simplex virus-2, on viral shedding and lesions: results of a randomized placebo-controlled trial. J Infect Dis 2018;218:1890–9.
15. Bernstein DI, Wald A, Warren T, Fife K, Tyring S, Lee P, et al. Therapeutic vaccine for genital herpes simplex virus-2 infection: findings from a randomized trial. J Infect Dis 2017;215:856–64.
16. Bernstein DI, Flechtner JB, McNeil LK, Heineman T, Oliphant T, Tasker S, et al. Therapeutic HSV-2 vaccine decreases recurrent virus shedding and recurrent genital herpes disease. Vaccine 2019;37:3443–50.
17. Jurtz V, Paul S, Andreatta M, Marcatili P, Peters B, Nielsen M. NetMHCpan-4.0: improved peptide-MHC class I interaction predictions integrating eluted ligand and peptide binding affinity data. J Immunol 2017;199:3360–8.
18. Castle JC, Kreiter S, Diekmann J, Lower M, van de Roemer N, de Graaf J, et al. Exploiting the mutanome for tumor vaccination. Cancer Res 2012;72:1081–91.
19. Mosely SI, Prime JE, Sainson RC, Koopmann JO, Wang DY, Greenawalt DM, et al. Rational selection of syngeneic preclinical tumor models for immunotherapeutic drug discovery. Cancer Immunol Res 2017;5:29–41.
20. Bloom MB, Perry-Lalley D, Robbins PF, Li Y, el-Gamil M, Rosenberg SA, et al. Identification of tyrosinase-related protein 2 as a tumor rejection antigen for the B16 melanoma. J Exp Med 1997;185:453–9.
21. Kuai R, Ochyl LJ, Bahjat KS, Schwendeman A, Moon JJ. Designer vaccine nanodiscs for personalized cancer immunotherapy. Nat Mater 2017;16:489–96.
22. Lee CH, Yelensky R, Jooss K, Chan TA. Update on tumor neoantigens and their utility: why it is good to be different. Trends Immunol 2018;39:536–48.
23. Linette GP, Carreno BM. Tumor-infiltrating lymphocytes in the checkpoint inhibitor era. Curr Hematol Malig Rep 2019;14:286–91.
24. Long D, Skoberne M, Gierahn TM, Larson S, Price JA, Clemens V, et al. Identification of novel virus-specific antigens by CD4(+) and CD8(+) T cells from asymptomatic HSV-2 seropositive and seronegative donors. Virology 2014;464–465:296–311.
25. Picard MD, Cohane KP, Gierahn TM, Higgins DE, Flechtner JB. High-throughput proteomic screening identifies Chlamydia trachomatis antigens that are capable of eliciting T cell and antibody responses that provide protection against vaginal challenge. Vaccine 2012;30:4387–93.
26. Moffitt KL, Gierahn TM, Lu YJ, Gouveia P, Alderson M, Flechtner JB, et al. T(H)17-based vaccine design for prevention of Streptococcus pneumoniae colonization. Cell Host Microbe 2011;9:158–65.
27. Davies DH, Duffy P, Bodmer JL, Felgner PL, Doolan DL. Large screen approaches to identify novel malaria vaccine candidates. Vaccine 2015;33:7496–505.
28. Gros A, Parkhurst MR, Tran E, Pasetto A, Robbins PF, Ilyas S, et al. Prospective identification of neoantigen-specific lymphocytes in the peripheral blood of melanoma patients. Nat Med 2016;22:433–8.
29. Tran E, Turcotte S, Gros A, Robbins PF, Lu YC, Dudley ME, et al. Cancer immunotherapy based on mutation-specific CD4+ T cells in a patient with epithelial cancer. Science 2014;344:641–5.
30. Hopewell EL, Cox C, Pilon-Thomas S, Kelley LL. Tumor-infiltrating lymphocytes: streamlining a complex manufacturing process. Cytotherapy 2019;21:307–14.
31. Bentzen AK, Marquard AM, Lyngaa R, Saini SK, Ramskov S, Donia M, et al. Large-scale detection of antigen-specific T cells using peptide-MHC-I multimers labeled with DNA barcodes. Nat Biotechnol 2016;34:1037–45.
32. Karosiene E, Rasmussen M, Blicher T, Lund O, Buus S, Nielsen M. NetMHCIIpan-3.0, a common pan-specific MHC class II prediction method including all three human MHC class II isotypes, HLA-DR, HLA-DP and HLA-DQ. Immunogenetics 2013;65:711–24.
33. van Rooij N, van Buuren MM, Philips D, Velds A, Toebes M, Heemskerk B, et al. Tumor exome analysis reveals neoantigen-specific T-cell reactivity in an ipilimumab-responsive melanoma. J Clin Oncol 2013;31:e439–42.
34. Ebrahimi-Nik H, Michaux J, Corwin WL, Keller GL, Shcheglova T, Pak H, et al. Mass spectrometry driven exploration reveals nuances of neoepitope-driven tumor rejection. JCI Insight 2019;5:e129152.
35. Richters MM, Xia H, Campbell KM, Gillanders WE, Griffith OL, Griffith M. Best practices for bioinformatic characterization of neoantigens for clinical utility. Genome Med 2019;11:56.
36. Bulik-Sullivan B, Busby J, Palmer CD, Davis MJ, Murphy T, Clark A, et al. Deep learning using tumor HLA peptide mass spectrometry datasets improves neoantigen identification. Nat Biotechnol 2019;37:55–63.
37. Abelin JG, Keskin DB, Sarkizova S, Hartigan CR, Zhang W, Sidney J, et al. Mass spectrometry profiling of HLA-associated peptidomes in mono-allelic cells enables more accurate epitope prediction. Immunity 2017;46:315–26.
38. Dowal L, Lyubetskaya A, Cabral C, Croll M, Warren C, Perry J, et al. Abstract LB-223: ATLAS™ reveals a dominant inhibitory antigen in melanoma patients, and a reduced breadth of tumor-associated antigen-specific T cells in non-responders to checkpoint blockade [abstract]. In: Proceedings of the Annual Meeting of the American Association for Cancer Research 2019; 2019 Mar 29–Apr 3; Atlanta, GA. Philadelphia (PA): AACR; 2019. p LB-223.

39. Kaufmann JK, Liu B, Jacques J, Wu N, Yan Z, Alami A, et al. Systematic analysis of T cell responses specific to the Epstein-Barr virus proteome using ATLAS™. J Immunol 2017;198:78.42.
40. Toes RE, Offringa R, Blom RJ, Melief CJ, Kast WM. Peptide vaccination can lead to enhanced tumor growth through specific T-cell tolerance induction. Proc Natl Acad Sci U S A 1996;93:7855–60.
41. Toes RE, Blom RJ, Offringa R, Kast WM, Melief CJ. Enhanced tumor outgrowth after peptide vaccination. Functional deletion of tumor-specific CTL induced by peptide vaccination can lead to the inability to reject tumors. J Immunol 1996;156:3911–8.
42. Vignali DA, Collison LW, Workman CJ. How regulatory T cells work. Nat Rev Immunol 2008;8:523–32.
43. Mellor AL, Lemos H, Huang L. Indoleamine 2,3-dioxygenase and tolerance: where are we now? Front Immunol 2017;8:1360.
44. Xia A, Zhang Y, Xu J, Yin T, Lu XJ. T cell dysfunction in cancer immunity and immunotherapy. Front Immunol 2019;10:1719.
45. Schade AE, Schieven GL, Townsend R, Jankowska AM, Susulic V, Zhang R, et al. Dasatinib, a small-molecule protein tyrosine kinase inhibitor, inhibits T-cell activation and proliferation. Blood 2008;111:1366–77.
46. Keskin DB, Anandappa AJ, Sun J, Tirosh I, Mathewson ND, Li S, et al. Neoantigen vaccine generates intratumoral T cell responses in phase Ib glioblastoma trial. Nature 2019;565:234–9.
47. Sabio E, Chan TA. The good, the bad, and the ugly: hyperprogression in cancer patients following immune checkpoint therapy. Genome Med 2019;11:43.
48. Kamada T, Togashi Y, Tay C, Ha D, Sasaki A, Nakamura Y, et al. PD-1(+) regulatory T cells amplified by PD-1 blockade promote hyperprogression of cancer. Proc Natl Acad Sci U S A 2019;116:9999–10008.
49. Li Y, Gierahn T, Thompson CM, Trzcinski K, Ford CB, Croucher N, et al. Distinct effects on diversifying selection by two mechanisms of immunity against Streptococcus pneumoniae. PLoS Pathog 2012;8:e1002989.
50. Russell AN, Zheng X, O'Connell CM, Wiesenfeld HC, Hillier SL, Taylor BD, et al. Identification of chlamydia trachomatis antigens recognized by T cells from highly exposed women who limit or resist genital tract infection. J Infect Dis 2016;214:1884–92.
51. Power CA, Grand CL, Ismail N, Peters NC, Yurkowski DP, Bretscher PA. A valid ELISPOT assay for enumeration of ex vivo, antigen-specific, IFNgamma-producing T cells. J Immunol Methods 1999;227:99–107.
52. Miyahira Y, Murata K, Rodriguez D, Rodriguez JR, Esteban M, Rodrigues MM, et al. Quantification of antigen specific CD8+ T cells using an ELISPOT assay. J Immunol Methods 1995;181:45–54.
53. Moodie Z, Price L, Gouttefangeas C, Mander A, Janetzki S, Lower M, et al. Response definition criteria for ELISPOT assays revisited. Cancer Immunol Immunother 2010;59:1489–501.